Available online at www.sciencedirect.com
ScienceDirect
Thin Solid Films 515 (2006) 1664 – 1673
www.elsevier.com/locate/tsf

Atomic layer deposition of palladium films on Al_2O_3 surfaces

J.W. Elam [a,*], A. Zinovev [b], C.Y. Han [b], H.H. Wang [b], U. Welp [b], J.N. Hryn [a], M.J. Pellin [b]

[a] Energy Systems Division, Argonne National Laboratory, Argonne, IL 60439, USA
[b] Materials Science Division, Argonne National Laboratory, Argonne, IL 60439, USA

Received 25 February 2005; received in revised form 25 May 2006; accepted 31 May 2006
Available online 18 July 2006

Abstract

We examined the atomic layer deposition (ALD) of Pd films using sequential exposures of Pd(II) hexafluoroacetylacetonate (Pd(hfac)$_2$) and formalin and discovered that formalin enables the efficient nucleation of Pd ALD on Al_2O_3. *In situ* quartz crystal microbalance measurements revealed that the Pd nucleation is hampered by the relatively slow reaction of the adsorbed Pd(hfac)$_2$ species, but is accelerated using larger initial Pd(hfac)$_2$ and formalin exposures. Pd nucleation proceeds via coalescence of islands and leaves hfac contamination at the Al_2O_3 interface. Pd films were deposited on the thermal oxide of silicon, glass and mesoporous anodic alumina following the ALD of a thin Al_2O_3 seed layer and analyzed using a variety of techniques. We measured a Pd ALD growth rate of 0.2 Å/cycle following a nucleation period of slower growth. The deposited films are cubic Pd with a roughness of 4.2 nm and a resistivity of 11 μΩ cm at 42 nm thickness. Using this method, Pd deposits conformally on the inside of mesoporous anodic alumina membranes with aspect ratio ~1500 yielding promising hydrogen sensors.

Keywords: Atomic layer deposition; Palladium; Formalin; Anodic aluminum oxide

1. Introduction

Pd metal has applications in hydrogen sensing [1–9], storage [7,10], and generation [11], as well as in catalysis [12]. For most of these applications, it is cost-effective to apply this precious metal as an ultrathin film. In addition, it is desirable to deposit Pd thin films on nanoporous materials to make responsive sensors [1,10,12,13] and efficient catalysts [12]. Atomic layer deposition (ALD) has been demonstrated to produce conformal films of a variety of materials including some metals with exquisite thickness control by utilizing alternating reactions between gaseous precursor molecules and a solid surface to deposit material in a layer-by-layer fashion. The chemical reactions terminate following the deposition of exactly one monolayer of adsorbed species so that the film thickness is easily controlled by the number of reaction cycles.

Pd has been deposited on oxides by ALD previously with limited success [14–16]. The difficulty has been the lack of metalorganic chemisorption on oxide terminated surfaces [17]. This difficulty has been used to advantage to produce nanoparticle Pd growth on alumina [15] and has been circumvented by pretreating the oxide surface with sulfide terminated silanes [16]. Pd ALD has also been accomplished using a hydrogen plasma as the reducing agent [18,19], however this method is not suitable to coating nanoporous substrates because of the rapid recombination of hydrogen radicals. Consequently, this investigation sought to find a method to nucleate and grow continuous Pd films directly on oxide surfaces including nanoporous membranes using ALD. It turns out that alternating exposures to Pd(II) hexafluoroacetylacetonate (Pd(hfac)$_2$) and formalin readily nucleates Pd on an Al_2O_3 surface. Because Al_2O_3 ALD films can be deposited on nearly any surface including oxides, metals, and polymers, the present method should allow Pd films to be easily deposited on any of these surfaces. Formalin has been used previously as a reducing agent in ALD Cu [20].

In this study, we use *in situ* quartz crystal microbalance (QCM) measurements to screen potential reducing agents for Pd ALD that allow nucleation on the ALD Al_2O_3 surface. These measurements identified formalin as an effective reducing agent for Pd ALD. Additional QCM measurements established the optimal timing sequence for the Pd ALD growth cycles and determined the effects of varying the ALD timing sequence on

* Corresponding author.
E-mail address: jelam@anl.gov (J.W. Elam).

0040-6090/$ - see front matter © 2006 Elsevier B.V. All rights reserved.
doi:10.1016/j.tsf.2006.05.049

the Pd nucleation. Following the QCM studies, Pd films were deposited on glass and Si substrates that had been coated with a 1–10 nm ALD Al_2O_3 seed layer. The properties of these films were studied using optical absorption, X-ray photoelectron spectroscopy (XPS), scanning electron microscopy (SEM), X-ray diffraction (XRD), atomic force microscopy (AFM) and four-point probe resistance measurements. Finally, ALD Pd films were deposited onto mesoporous anodic aluminum oxide (AAO) membranes with an aspect ratio of pore length/pore diameter $L/d \sim 1500$. Complete penetration of the Pd films into the very high aspect ratio membranes was confirmed using cross sectional energy dispersive analysis of X-ray (EDAX) measurements. Preliminary hydrogen sensing measurements were performed on the Pd/AAO membranes.

2. Experimental details

The ALD utilized a viscous flow reactor that is similar to previous systems [21]. Briefly, a stainless steel flow tube with an inside diameter of 5 cm houses substrates for film growth as well as the QCM. Ultrahigh purity nitrogen carrier gas continuously passes through the flow tube at a mass flow rate of 200 sccm and a pressure of 1 Torr. A constant reactor temperature is maintained by four separate temperature controllers connected to resistive heating elements attached to the outside of the reactor. The four heating zones create a uniform temperature profile along the length of the flow tube to reduce the influence of temperature transients on the QCM measurements [22].

Palladium ALD was performed using alternating exposures to Pd(II) hexafluoroacetylacetonate ($Pd(hfac)_2$) and formalin, both obtained from the Aldrich chemical company. Formalin consists of a 37% solution of formaldehyde in water containing 10–15% methanol to inhibit the formation of paraformaldehyde. Formaldehyde is toxic and potentially carcinogenic and should be handled carefully. The $Pd(hfac)_2$ is held in a stainless steel bubbler maintained at 50 °C. At this temperature, the $Pd(hfac)_2$ has a vapor pressure slightly less than 0.1 Torr [23]. The tubing connecting the bubbler to the ALD reactor is held at 100 °C to prevent the readsorption of the $Pd(hfac)_2$. Ultrahigh purity nitrogen (99.999%) at a mass flow rate of 50 sccm was sent through the bubbler during the $Pd(hfac)_2$ exposures, and was diverted to bypass the bubbler following the $Pd(hfac)_2$ exposures. This switching was accomplished using computer-controlled pneumatic diaphragm valves.

Prior to the Pd ALD, an ALD Al_2O_3 film with a thickness of 1–10 nm was deposited first as a buffer or seed layer. The Al_2O_3 ALD was performed using alternating exposures to trimethyl aluminum (TMA, Aldrich Chemical Company) and deionized water at 200 °C. The TMA, H_2O and formalin precursors were introduced into the reactor via computer-controlled pneumatic diaphragm valves and metering valves were used to adjust the flow rate of the precursors during the exposures to ~20 sccm [21]. The ALD timing sequences can be expressed as t_1–t_2–t_3–t_4 where t_1 is the exposure time for the first precursor, t_2 is the purge time following the first exposure, t_3 is the exposure time for the second precursor, t_4 is the purge time following the exposure to the second precursor and all units are given in seconds (s). The timing sequence for Al_2O_3 ALD was 1–5–1–5 s while the Pd ALD timing sequence was typically 1–1–1–1 s.

A QCM could be installed in the ALD reactor enabling *in situ* measurements during the Pd and Al_2O_3 growth. These measurements utilized a Maxtek BSH-150 bakeable sensor and AT-cut quartz sensor crystals with a polished front surface obtained from the Colorado Crystal Corporation, Part # CCAT1BK-1007-000. The QCM measurements were made using a Maxtek TM400 film thickness monitor interfaced to a personal computer.

Pd ALD films were deposited on 2 cm × 2 cm Si(111) and glass substrates. Prior to loading, the substrates were ultrasonically cleaned in acetone and then methanol and blown dry using nitrogen. After loading, the substrates were allowed to outgas in the ALD reactor for 10 min at 200 °C in 1 Torr of flowing ultrahigh purity nitrogen. Next, the substrates were cleaned *in situ* using a 60 s exposure to 10% ozone in oxygen at a pressure of 2 Torr and a mass flow rate of 400 sccm. The SEM images were acquired using a Hitachi S4700 SEM with a field emission gun electron beam source and an EDAX detector for elemental analysis. The AFM measurements used a digital instrument Dimension 3000 with a NanoScope IIIa controller operated in tapping mode. XRD measurements used a Rigaku Miniflex Plus diffractometer. Optical absorption measurements were performed on ALD Pd films deposited on glass slides using a J. A. Woolam Co. M2000 spectroscopic ellipsometer operated in transmission mode, and the absorption spectra were fit to a model using Pd optical constants supplied with the instrument to obtain the Pd film thickness. XPS measurements were made using MgKα (1253.6 eV) radiation and a hemispherical electron energy analyzer.

AAO membranes with hexagonally ordered arrays of nanopores were prepared by a two-step anodization procedure as described previously [24,25]. Aluminum sheets (Alfa Aesar, 99.998% pure, 0.5 mm thick) were degreased in acetone and then annealed at 500 °C for 4 h under an argon atmosphere. The Al sheets were then electropolished in a solution of $HClO_4$ and ethanol (1:8, v/v) at a current density of 200 mA/cm^2 for 10 min or until a smooth, mirror-like surface was achieved. The first anodization step was carried out in a 0.3 M oxalic acid solution at 3 °C for 24 h. The 70 μm thick porous alumina layer was then stripped away from the Al substrate by etching the sample in a solution containing 6 wt.% phosphoric acid and 1.8 wt.% chromic acid at 60 °C for 12 h. This step not only removes the disordered AAO membrane but also leaves a highly ordered dimple array on the aluminum surface. Each dimple initiates new pore formation during the second anodization step, which was carried out under the same conditions as the first step. A freestanding AAO membrane with highly ordered arrays of nanopores was obtained by selectively etching away the unreacted Al in saturated $HgCl_2$ solution. The membrane was then immersed in 5.00 wt.% phosphoric acid at 30.0 °C for 65 min to remove the barrier layer.

The AAO membranes were first coated by a buffer layer of Al_2O_3 using 9 TMA/H_2O ALD cycles with the timing sequence

10–20–10–20 s. Next, the AAO was coated with Pd using 118 Pd(hfac)$_2$/formalin cycles with the timing sequence 20–5–20–5 s. These very long ALD exposures were necessary to ensure the complete penetration of the ALD precursors into the extremely high aspect ratio AAO pores, and the exposure times were calculated using a formula derived from a diffusional model [26]. The coated AAO membranes were examined using SEM, cross sectional EDAX and electrical conductivity. For the electrical conductivity measurements, Pd-contacts with ~30 nm thickness were deposited onto the sample using thermal evaporation through a shadow mask. 50 μm gold wires were attached to these contacts with silver paint, and the sample was mounted into a small aluminum gas flow cell. Changes in sample resistance upon hydrogen exposure were monitored using standard lock-in techniques with a drive current of 10 μA at a frequency of 23 Hz.

3. Results and discussion

3.1. Nucleation of Pd on Al_2O_3

The nucleation of Pd on Al_2O_3 was investigated by first depositing a 10 nm Al_2O_3 ALD buffer layer on the QCM using alternating TMA/H_2O exposures and subsequently attempting to deposit Pd using Pd(hfac)$_2$ and various reducing agents. The reducing agents investigated were H_2 (>99.99%), methanol (99.9%), ethanol (>99.5%), isopropanol (99.9%), acetone (>97.5%), TMA [27] (97%), and formalin. Several oxidizing agents were also explored with the idea of initially depositing PdO films and then subsequently reducing to metallic Pd using H_2 as has been demonstrated for ALD Ni [28]. The oxidizing agents evaluated were hydrogen peroxide (30% in H_2O), water (deionized, >18 MΩ cm), oxygen (99.999%) and ozone (~10% in oxygen). These Pd and PdO ALD experiments primarily used the timing sequence 1–5–1–5 s, however longer exposure times were also investigated. Of all the chemical species screened, only formalin effectively nucleated Pd ALD on Al_2O_3 surfaces. Although H_2 has been used previously to deposit ALD Pd films on Ir [16], our measurements revealed that H_2 is not effective for nucleating Pd growth on Al_2O_3. Even after many hundreds of Pd(hfac)$_2$/H_2 cycles at temperatures between 100 and 200 °C, no growth was observed by QCM. The Pd ALD nucleation using formalin was only effective at 200 °C and did not occur at 100 °C. However, once the Pd had nucleated, either formalin or H_2 could be used for subsequent Pd ALD at either 100 or 200 °C and the growth rates determined from the QCM measurements were identical. Temperatures above 200 °C and below 100 °C were not explored because Pd(hfac)$_2$ begins to decompose at 230 °C [23] and was vaporized at 50 °C.

Simple chemical arguments can rationalize the success of formalin for nucleating Pd growth on Al_2O_3. We assume that formaldehyde (HCOH) is the active reducing agent in the formalin solution because both H_2O and methanol did not nucleate the Pd growth when tested individually. Although H_2 can be a powerful reducing agent, either high temperatures or a catalytic surface (e.g. Pd, Ir) is required to break the dihydrogen bond. In contrast, HCOH can provide H atoms for Pd reduction at lower temperatures if the formaldehyde is bound for a sufficient time to allow decomposition. The polar carbonyl (CO) group of formaldehyde generates a relatively large dipole moment of 2.33 D (Debye) vs. 0 D for H_2 and 1.66–1.70 D for the alcohols. Consequently, strong dipole–dipole interaction between formaldehyde and the polar Pd(hfac)* surface species may provide sufficient binding to allow HCOH decomposition. Although acetone also has a large dipole moment (2.88 D), the absence of H atoms bound directly to the carbonyl makes acetone a weaker reducing agent. It is also possible that the water in the formalin may partially decompose the Pd(hfac)* ligands thereby exposing new adsorption sites for additional Pd (hfac)$_2$ molecules. However, this cannot be the sole mechanism for Pd nucleation on Al_2O_3 since alternating Pd(hfac)$_2$/H_2O exposures yielded no growth. Perhaps it is not surprising that formalin facilitates Pd nucleation given that this is a common reducing agent in electroless plating [29]. Further *in situ* measurements using XPS and quadrupole mass spectrometry [30] might clarify the role of the HCOH.

The influence of the Pd ALD timing sequence on the nucleation was examined by first depositing a 10 nm Al_2O_3 ALD buffer layer on the QCM and subsequently depositing Pd using Pd(hfac)$_2$/formalin with the different timing sequences given in Fig. 1. For these experiments, the timing sequence was adjusted to be 1–1–1–1 s following the deposition of ~1 Pd monolayer. The QCM measurements in Figs. 1, 3 and 4) assume a Pd density of 12.0 g/cm^3. Fig. 1 reveals that using the 1–1–1–1 s timing sequence, the Pd growth rate is lower initially on the Al_2O_3 surface and then gradually increases to reach the steady-state growth rate of 0.21 Å/cycle following ~140 Pd ALD cycles. Approximately 100 cycles are needed to deposit 1 Pd monolayer using the 1–1–1–1 s timing sequence. This ~140 cycle nucleation period may produce rough or

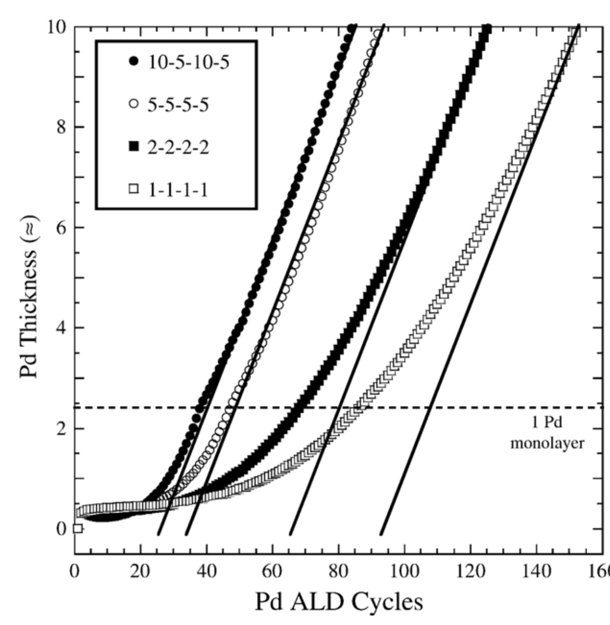

Fig. 1. Nucleation of Pd on Al_2O_3 using different Pd ALD timing sequences measured by *in situ* QCM. In each of the four measurements, the Pd ALD timing sequence was adjusted to 1–1–1–1 s following the deposition of 1 Pd monolayer.

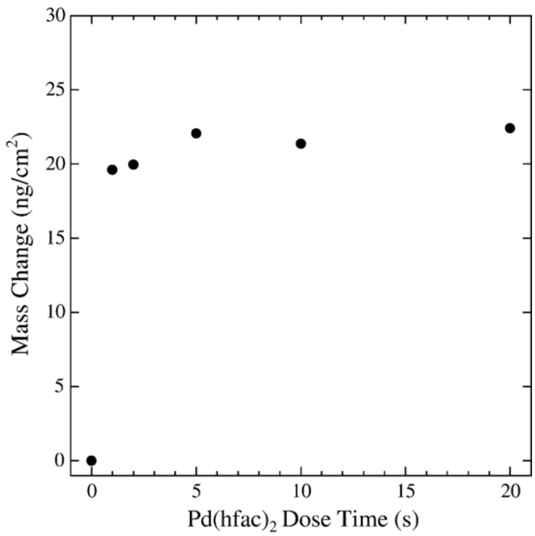

Fig. 2. Mass gain from initial $Pd(hfac)_2$ exposure on Al_2O_3 vs. $Pd(hfac)_2$ exposure time.

discontinuous films due to 3-dimensional island growth. Fortunately, the Pd ALD can be accelerated using larger initial $Pd(hfac)_2$ and formalin exposures. Using the 10–5–10–5 s sequence, the steady-state growth rate is achieved in only 30 cycles and 35 cycles are required to deposit 1 Pd monolayer. The Pd nucleation was not greatly accelerated by increasing just the $Pd(hfac)_2$ or the formalin exposure alone (e.g. 10–5–1–1 s or 1–1–10–5 s), indicating that the reactivity of both precursors is diminished on the Al_2O_3 surface as compared with the Pd surface. The faster nucleation observed using longer initial Pd ALD exposures may result, in part, from a higher Pd growth rate. Accelerated nucleation using larger initial exposures has been observed previously for ALD W on SiO_2 [31] and Al_2O_3 [32].

Fig. 2 shows the mass deposited on the Al_2O_3-coated QCM surface during the initial $Pd(hfac)_2$ exposure as a function of the exposure time. This figure demonstrates that $Pd(hfac)_2$ reacts readily with the Al_2O_3 surface and the coverage saturates at ~20 ng/cm^2 even after very short $Pd(hfac)_2$ exposures of only 1 s. This reaction is likely to be:

$$\text{Al–OH}^* + \text{Pd(hfac)}_2 \rightarrow \text{Al–O–Pd(hfac)}^* + \text{Hhfac} \quad (1)$$

Where the asterisks designate surface species. The hfac ligand that is removed from the $Pd(hfac)_2$ molecule may leave as Hfac vapor as shown in Eq. (1), or may anchor to the Al_2O_3 surface on an adjacent Al–O–Al site. Given that the nucleation of Pd ALD on the Al_2O_3 surface is slow and requires repeated, large exposures to both $Pd(hfac)_2$ and formalin, it is puzzling that the very first reaction of the $Pd(hfac)_2$ precursor on Al_2O_3 is so rapid. $Pd(hfac)_2$ has been shown to bond strongly to alumina with both hfac ligands remaining on the surface [33], and this would explain the relatively large mass increase in Fig. 2. Moreover, strong bonding between $Pd(hfac)_2$ and Al_2O_3 surface would explain the fast initial reactivity in Fig. 2. The much slower nucleation following this initial adsorption may reflect the lower reactivity of the partially oxidized Al–O–Pd(hfac)* surface when compared with the Pd(hfac)* surface formed when $Pd(hfac)_2$ reacts with Pd.

To further explore the Pd nucleation, ALD Pd films were deposited using the timing sequence 2–2–1–2 s on Si(111) substrates and subsequently examined using XPS and SEM. Prior to Pd ALD, the substrates were coated with an ALD Al_2O_3 buffer layer using 20 TMA/H_2O cycles at 200 °C with the timing 1–5–1–5 s. Samples were immediately transferred into the XPS analysis chamber after deposition to minimize contamination. Fig. 3 shows XPS spectra recorded from Pd films with thicknesses of 13 and 51 Å as determined from optical absorption measurements of Pd films deposited concurrently on glass. The Pd 3d peak for the 51 Å sample appears at 335.6 eV as expected for metallic Pd, but at 337.1 eV for the 13 Å sample. This higher binding energy for the thinner sample is indicative of oxidized Pd suggesting that much of the Pd is bound to substrate oxygen in agreement with Eq. (1). Fluorine and aluminum are detected on both samples, and these elements may exist underneath the thin Pd film or on regions of

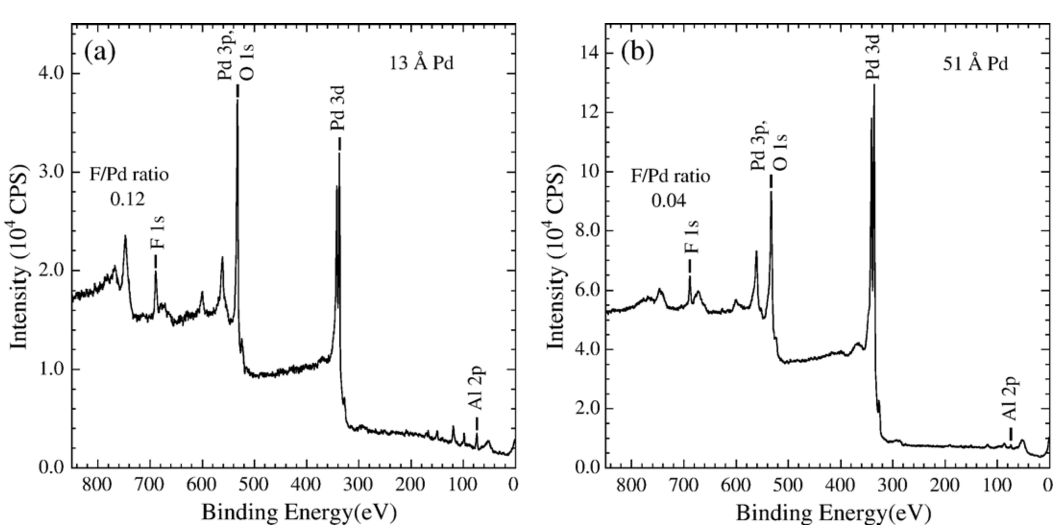

Fig. 3. XPS spectra for (a) 13 and (b) 51 Å Pd films deposited on Al_2O_3.

the Al_2O_3 surface that are not yet coated by Pd. The absolute intensity for the F 1s and Al 2p peaks remains nearly constant within a factor of 2 as the Pd thickness increases from 13 to 51 Å. This finding suggests that the F and Al reside at uncoated regions of the Al_2O_3 surface. If the F and Al existed below Pd films of thickness 13 and 51 Å in Fig. 3a and b, then the XPS signals for these elements would be attenuated by $\exp(-\Delta T/\lambda)=0.02$ for F and 0.08 for Al where $\Delta T=38$ Å is the Pd thickness change and λ is the inelastic mean free path for the F 1s ($\lambda=10$ Å) and Al 2p electrons ($\lambda=15$ Å) [34]. In agreement with this observation, angle-dependent XPS measurements performed on these samples revealed little change in the F/Pd signal ratio as the detection angle increased from normal incidence to 70°, indicating that the F and Pd are both located on the surface. The peak at 532.6 eV is an unresolved feature from Pd $3p_{3/2}$ and O 1s where the O signal originates from both Al_2O_3 and hfac ligands.

Taken together, the XPS results suggest that some hfac ligands remain bound to the Al_2O_3 surface and are neither removed by the formalin nor covered with Pd, at least for these thinner Pd films. Furthermore, the nearly constant Al signal indicates that the Al_2O_3 substrate surface is not yet totally covered by Pd. Presumably carbon is also present on the surface but our XPS sensitivity to carbon is low and we failed to detect carbon in any of these samples. It should be noted that the F/Pd ratio measured for the 51 Å Pd film is comparable to that observed previously for ALD Pd films of similar thickness deposited onto Ir at 80 °C using alternating $Pd(hfac)_2/H_2$ exposures [16]. In contrast, no F was detected previously for Pd films deposited using hydrogen radicals [18]. Evidently, the very reactive hydrogen radicals are necessary to completely remove F from the interface.

Fig. 4 presents SEM images of Pd films with thicknesses of 2.7, 13, 36 and 54 Å. The Pd deposits as discrete islands that grow laterally with increasing Pd ALD cycles and eventually coalesce. The gaps between the islands are likely to be Al_2O_3 that is partially coated by hfac ligands so as to present F and Al signal in the XPS measurements and possibly block the adsorption of additional $Pd(hfac)_2$ molecules thereby inhibiting nucleation. The density of Pd islands measured from these images is $\sim 1\times 10^{12}$ cm^{-2} and remains nearly constant with increasing thickness suggesting that no new islands are forming. The Pd islands probably nucleate around the initial Pd atoms that bind to the Al_2O_3 surface during the very first $Pd(hfac)_2$ exposure. The number density of these initial Pd atoms calculated from the QCM mass change in Fig. 2 is 1.3×10^{13} cm^{-2}. This value is $\sim$10× larger than the density of Pd islands observed in the SEM images suggesting that only 10% of the initial Pd atoms are active for Pd film nucleation. As shown in Fig. 1, the Pd nucleation rate is enhanced using greater $Pd(hfac)_2$ and HCOH exposures. These greater exposures may activate a larger proportion of the initial Pd atoms. Alternatively, greater exposures may initiate new Pd islands via the attachment of $Pd(hfac)_2$ to additional, less favorable sites on the Al_2O_3 surface. In either case, the larger reactant exposures should reduce the number of Pd ALD cycles required to achieve coalescence yielding smoother, more continuous Pd films.

The XPS and SEM measurements reveal that the Pd nucleation on Al_2O_3 proceeds by island coalescence rather than ideal layer-by-layer growth and residual hfac ligands may contaminate the interface. Despite these shortcomings, the $Pd(hfac)_2$/formalin procedure is useful because it enables the metallization of nanoporous materials (*vide infra*). Furthermore, because Al_2O_3 ALD deposits readily on nearly any surface including oxides [35],

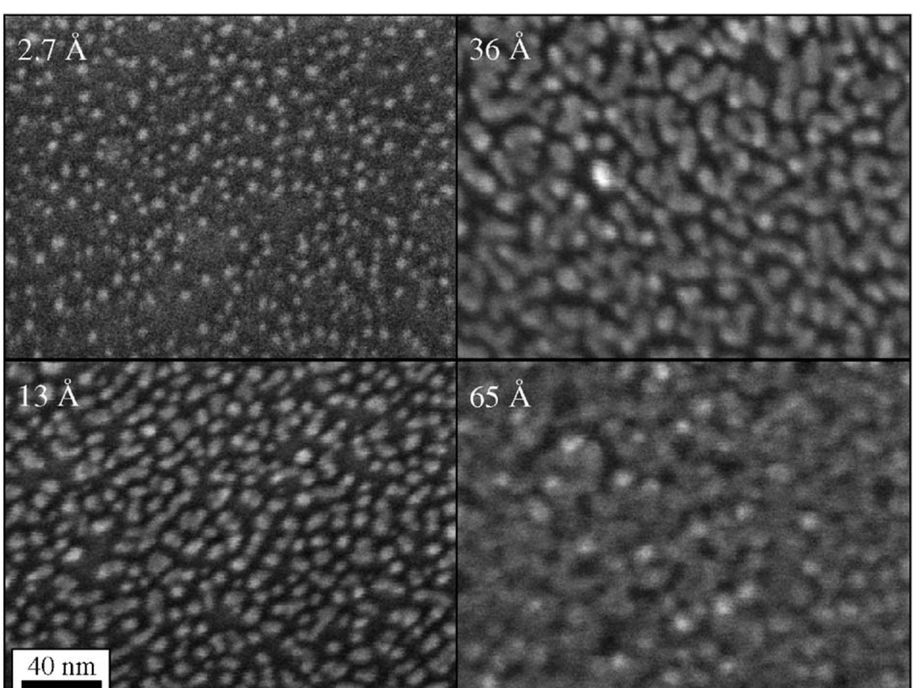

Fig. 4. SEM images of 2.7, 13, 36, and 65 Å Pd films deposited on Al_2O_3.

metals [36] and polymers [37], this nucleation technique will allow Pd to be deposited with atomic layer control on these surfaces after the deposition of a thin ALD Al_2O_3 seed layer. Formalin may allow Pd films to be deposited directly on other oxide surfaces without the need for an Al_2O_3 seed layer.

3.2. Growth of Pd

Following the nucleation studies, the QCM was used to determine the optimum timing sequence for Pd ALD. As shown in Fig. 5a, the Pd ALD growth rate increases rapidly with Pd(hfac)$_2$ exposure time and reaches 0.21 Å/cycle at $t_1=1$ s. The Pd growth rate continues to increase slowly for $t_1>1$ s and achieves 0.28 Å/cycle at $t_1=5$ s. This gradual saturation has been observed in other ALD systems [38] and may reflect a decreasing Pd(hfac)$_2$ reactivity with increasing surface coverage. In contrast to the Pd(hfac)$_2$ results, the Pd growth rate is completely saturated for formalin exposures exceeding 0.5 s (Fig. 5b). The Pd ALD growth rate changes very little with increasing Pd(hfac)$_2$ and formalin purge times exceeding 0.5 s (Fig. 5c, d). For the remaining studies, the timing sequence 1–1–1–1 s was used for the Pd ALD. Although this timing sequence is not completely saturated in the Pd(hfac)$_2$ exposures, it optimizes the Pd deposition rate in light of the relatively low ALD Pd growth rate of ~0.2 Å/cycle.

Fig. 6a shows QCM data obtained during Pd ALD using the 1–1–1–1 s timing sequence for 50 Pd ALD cycles on an already-deposited ALD Pd surface. The data shows highly linear growth at 0.21 Å/cycle. An expanded view of this data is shown in Fig. 6b to illustrate the QCM structure for the individual Pd ALD cycles. Information about the Pd ALD growth mechanism can be elucidated from Fig. 6b. One possible reaction sequence for Pd ALD is given by:

$$\mathrm{Pd{-}H}_x^* + \mathrm{Pd(hfac)}_2 \rightarrow \mathrm{Pd{-}Pd(hfac)}_{2-x}^* + x\mathrm{Hhfac} \quad (2)$$

$$\mathrm{Pd{-}Pd(hfac)}_{2-x}^* + \mathrm{HCOH} \rightarrow \mathrm{Pd{-}Pd{-}H}_x^* + 2-x\mathrm{Hhfac} + \mathrm{CO} \quad (3)$$

In reaction (2), one Pd(hfac)$_2$ molecule reacts with the H-terminated Pd surface to liberate x Hhfac molecules and

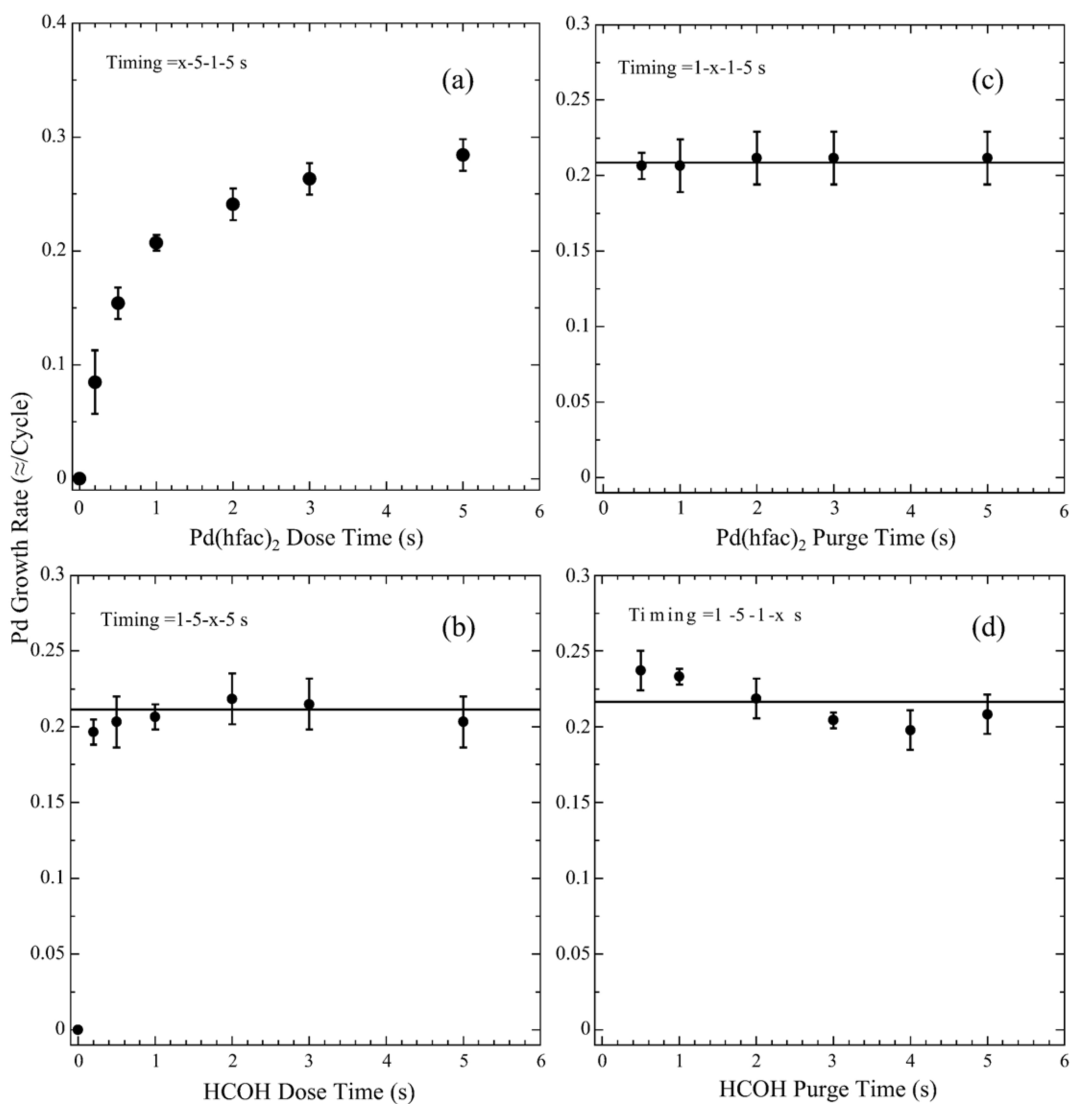

Fig. 5. Pd ALD growth rate measured by QCM for different Pd ALD timing sequences.

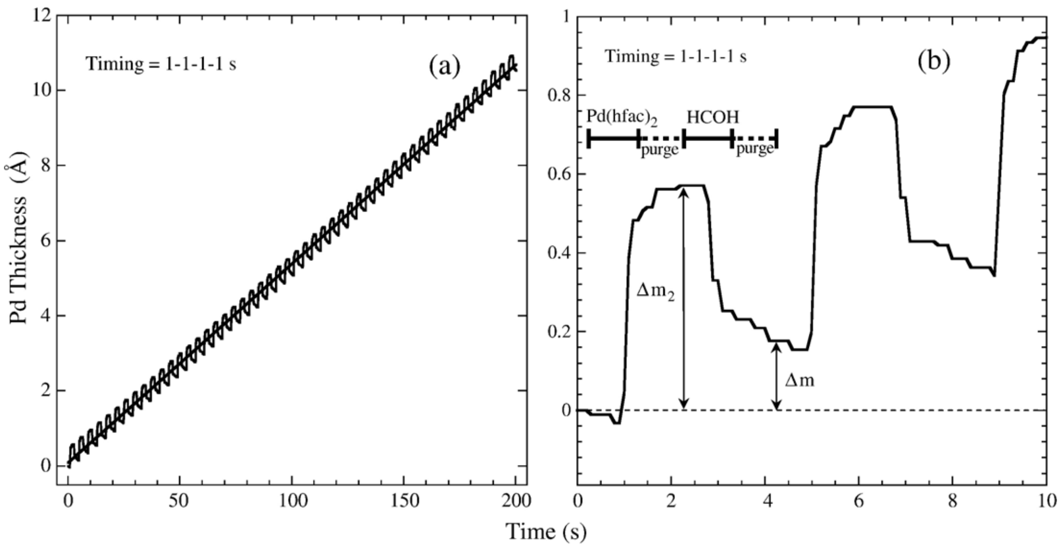

Fig. 6. (a) Pd ALD measured by QCM using 1–1–1–1 s timing sequence showing linear growth at 0.21 Å/cycle. (b) Expanded view of Pd ALD steps showing thickness increase during $Pd(hfac)_2$ exposures and thickness decrease during HCOH exposures.

deposit a new layer of Pd on the surface that is now hfac-terminated. In reaction (3), the newly generated Pd-hfac surface reacts with HCOH. The HCOH decomposes to form 2H and CO, and the H reacts with Pd–hfac to release the remaining $(2-x)$ hfac ligands and regenerate the starting surface. The number of hfac ligands released in each reaction is left variable to allow for different possible stoichiometries. The actual stoichiometry for the surface reactions can be determined from the QCM data using the relationship: $R=\Delta m/\Delta m_2$ where Δm is the mass change following one complete Pd ALD cycle and Δm_2 is the mass change during reaction (2). From Eqs. (2) and (3) and the atomic masses, $\Delta m=\mathrm{M(Pd)}=106$ and $\Delta m_2=\mathrm{M(Pd)}+(2-x)\mathrm{M(hfac)}-x\mathrm{M(H)}=520-208x$ so that $R=106/(520-208x)$. Because thickness is linearly related to mass on the QCM, R can be obtained from Fig. 6. Averaging over the 50 cycles shown in Fig. 6a, $\Delta m=0.21$ and $\Delta m_2=0.60$ so that $R=0.35$. Consequently, $x=1.0$ implying that one of the two hfac ligands is released from the surface during reaction (2).

The thickness of a Pd monolayer (ML) calculated from the bulk density of Pd is 2.45 Å. Therefore, the 0.21 Å/cycle Pd ALD growth rate derived from the QCM measurements is only ~0.1 ML. This slow growth rate may result from the bulky hfac ligand remaining on the Pd surface following the $Pd(hfac)_2$ exposure blocking the adsorption of additional $Pd(hfac)_2$ molecules. Alternatively, adsorption may occur only at isolated sites such as Pd dimers on the surface, and the limited number of these discrete sites may limit the growth rate. Additional support for the mechanism given by reactions (2) and (3) is that the QCM signals obtained using H_2 as the reducing agent when depositing Pd ALD on a Pd surface are identical to those using HCOH. This finding suggests that the HCOH serves merely as a hydrogen source as indicated in reaction (3). Additional *in situ* quadrupole mass spectrometer measurements [30] could identify the gaseous reaction products and clarify the growth mechanism.

3.3. Properties of Pd Films

After studying the Pd nucleation and growth, thicker Pd films were deposited on 2 nm ALD Al_2O_3 coatings on Si(111) wafers and glass slides using alternating $Pd(hfac)_2$/HCOH exposures at 200 °C with the timing sequence 1–1–1–1 s. Fig. 7 presents optical absorption and cross-sectional SEM measurements vs. number of Pd ALD cycles and shows a growth rate of 0.22 Å/Cycle in very good agreement with the QCM results. Because the QCM measurements assumed a density of 12.0 g/cm^3, this agreement indicates that the ALD Pd films are fully dense. Fig. 7 shows a nucleation period of several hundred cycles to reach the steady-state growth rate that also corroborates the QCM work.

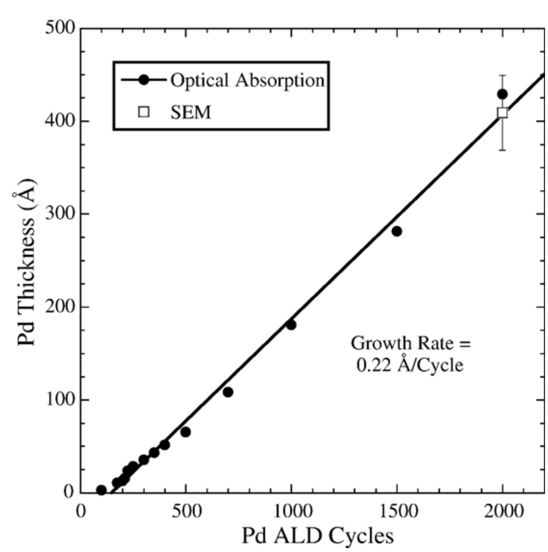

Fig. 7. Pd thickness vs. number of Pd ALD cycles measured using optical absorption of Pd films on glass (solid circles) and cross-sectional SEM of Pd films on Si(111) (open square).

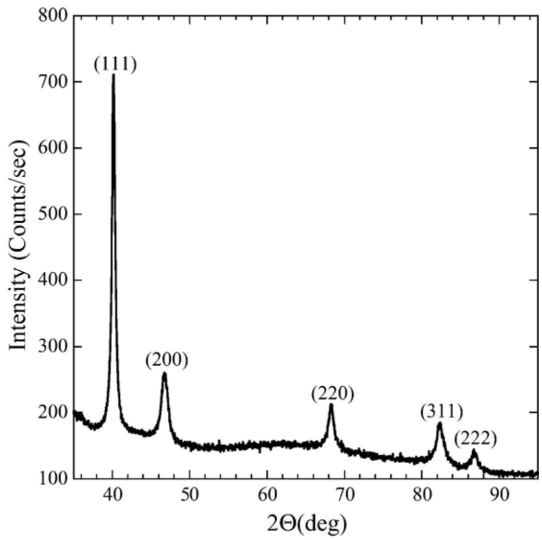

Fig. 8. XRD pattern for 80 nm ALD Pd film on glass.

XRD measurements of an 80 nm ALD Pd films deposited on glass (Fig. 8) reveals face-centered cubic Pd with a preferred <111> orientation using the peak assignments from JCDPS #89-4897 as has been observed previously for ALD noble metal films including Pd [14]. AFM analysis of a 42 nm Pd film on Si(111) (Fig. 9) shows a nanocrystalline morphology with a root mean squared (RMS) surface roughness of 4.2 nm. A similar surface roughness was measured for ALD Pt films of comparable thickness [39]. Fig. 10 shows an SEM image of the same 42 nm Pd film on Si (111) and reveals a nanocrystalline morphology that is consistent with the XRD and AFM observations. In contrast to the thinner films, XPS measurements of the 42 nm Pd ALD film revealed no fluorine contamination. Furthermore, the absence of substrate Al and O peaks demonstrates that the thick Pd films are continuous and pinhole-free within the instrumental sensitivity of ~1%.

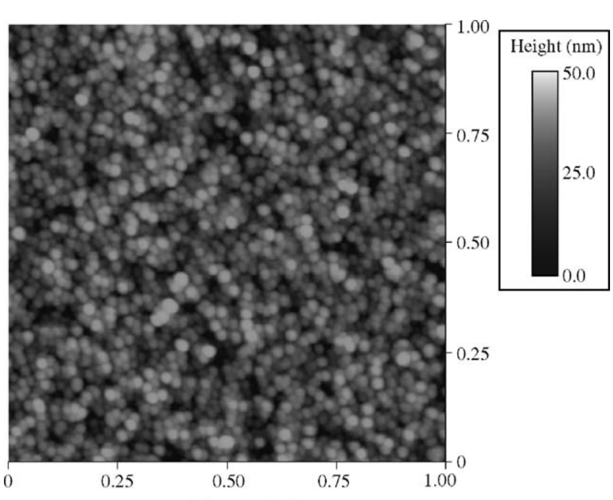

Fig. 9. Tapping mode AFM image from 42 nm ALD Pd film on Si(111). The RMS roughness is 4.2 nm.

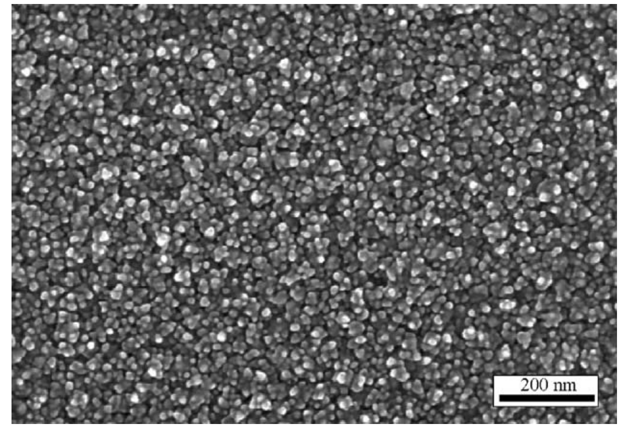

Fig. 10. SEM image of 42 nm ALD Pd film on Si(111).

The resistivity of the ALD Pd films deposited on glass decreased with increasing film thickness from 37 μΩ cm at 4 nm to 14 μΩ cm at 42 nm. This final value is only slightly higher than the accepted Pd bulk resistivity of 11 μΩ cm. The adhesion of the Pd films to glass and Si(111) substrates was fine for Pd film thicknesses below ~20 nm and no delamination was observed during scotch tape pull tests. Evidently the Pd is still well bonded to the Al_2O_3 surface despite interfacial contamination introduced during nucleation. Thicker films were partially removed from the substrates during testing suggesting higher stress in the thicker films. Depositing these >20 nm Pd films at a lower

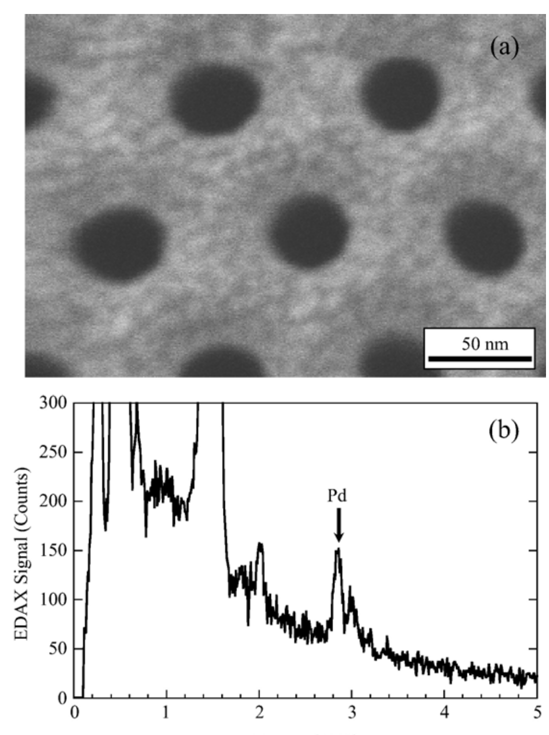

Fig. 11. (a) SEM image of high aspect ratio anodic aluminum oxide (AAO) membrane surface following deposition of ~2 nm ALD Pd. (b) EDAX spectrum recorded from middle of Pd-coated AAO membrane showing penetration of ALD Pd into center of pores.

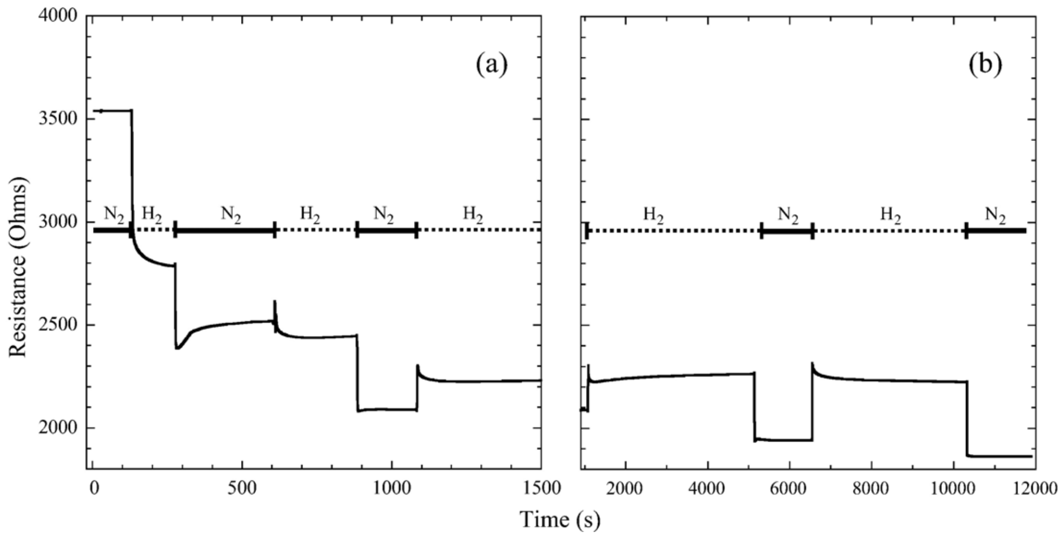

Fig. 12. Hydrogen sensitivity of ALD Pd-coated AAO membrane measured by resistance across membrane during alternating H_2 and N_2 exposures for short (a) and long (b) measurement times.

temperature of 100 °C might yield lower stress and better adhesion.

To demonstrate the ability to conformally coat very high aspect ratio substrates using Pd ALD, an AAO membrane with thickness $L=60$ µm and initial pore diameter $d=40$ nm was coated with ~2 nm ALD Pd. Fig. 11a presents an SEM image of the Pd-coated AAO membrane and reveals the same nanocrystalline morphology observed for the thicker Pd films deposited on Si(111) substrates. Fig. 11b shows an EDAX spectrum recorded from middle of the Pd-coated membrane demonstrating penetration of the Pd ALD into the center of the very high aspect ratio ($L/d\sim1500$) AAO pores.

The ALD Pd/AAO membranes show promise as hydrogen sensors. Fig. 12 plots the resistance across the surface of the membrane vs. time when exposed sequentially to 10 vol.% H_2 in N_2 and pure N_2. Upon first exposing the sample to hydrogen (Fig. 12a), the resistance drops significantly and irreversibly. This resistance drop may result from enhanced inter-granular contact following volume expansion to form the Pd-hydride [40,41]. Following the third exposure, the resistance changes becomes reproducible and stable (Fig. 12b). In this state, hydrogen exposure *increases* the resistance by about 20%. This value is in good agreement with previous measurements for continuous Pd films [42]. The time response for the Pd/AAO membrane is <1 s. Because the intrinsic hydrogen dissociation and diffusion times on nm-sized grains and films at room temperature are $\sim10^{-6}$ s, [40] the ~1 s time constant in Fig. 12 suggests that slow gas exchange in our flow cell limits the instrumental time response.

4. Conclusions

Pd films were deposited with atomic layer control at 200 °C on ALD Al_2O_3 surfaces using sequential $Pd(hfac)_2$/HCOH exposures. Because ALD Al_2O_3 films can be deposited readily on most surfaces, ALD Pd films can also be deposited on these surfaces by first applying a thin, ALD Al_2O_3 seed layer. Although the initial adsorption of $Pd(hfac)_2$ on Al_2O_3 is rapid, subsequent Pd growth is hampered by the relatively slow reduction of the adsorbed $Pd(hfac)_2$ species. Nucleation occurs via lateral spreading and coalescence of a relatively low density of Pd islands. However, nucleation is accelerated using larger initial $Pd(hfac)_2$/HCOH exposures. QCM measurements yield a Pd ALD growth rate of 0.2 Å or ~0.1 Pd monolayer per cycle. This low growth rate may result from site-blocking by hfac ligands.

Analysis of ALD Pd films deposited on Al_2O_3-coated Si (111) and glass substrates at 200 °C confirmed the 0.2 Å/cycle Pd growth rate following a nucleation period of slower growth. The Pd films exhibit an RMS roughness of 4.2 nm and deposit in the cubic phase. XPS measurements detect no impurities in thicker films, but fluorine is found at the Al_2O_3–Pd interface for thinner films. The Pd films are highly conductive with a resistivity of 14 µΩ cm. SEM and EDAX measurements demonstrate that this technique deposits conformal Pd films on the inside surfaces of mesoporous AAO membranes with an aspect ratio $L/d\sim1500$, and the resulting Pd/AAO structures show promise as hydrogen sensors.

Acknowledgements

The work at Argonne is supported by the U.S. Department of Energy, BES-Materials Sciences under Contract W-31-109-ENG-38.

References

[1] W. Jakubik, M. Urbanczyk, S. Kochowski, J. Bodzenta, Sens. Actuators, B 96 (2003) 321.
[2] P. Kumar, L. Malhotra, Mater. Chem. Phys. 88 (2004) 106.
[3] K. Lin, H. Chen, H. Chuang, C. Chen, C. Lu, C. Cheng, W. Liu, IEEE Sens. J. 4 (2004) 72.

[4] V. Litovchenko, A. Efremov, T. Gorbanyuk, Y. Ptushinskii, O. Kanach, V. Golovanov, A. Kiv, T. Rantala, Phys. Low-Dimens. Struct. 3–4 (2004) 17.
[5] R. O'Neill, S. Chang, J. Lowry, C. McNeil, Biosens. Bioelectron. 19 (2004) 1521.
[6] S. Roy, C. Jacob, S. Basu, Sens. Actuators, B 94 (2003) 298.
[7] Z. Sun, B. Shen, Rare Metal Mat. Eng. 33 (2004) 889.
[8] K. Yoshimura, Y. Yamada, M. Okada, M. Tazawa, P. Jin, Jpn. J. Appl. Phys. 43 (2004) L507.
[9] Z. Zhao, Y. Sevryugina, M. Carpenter, D. Welch, H. Xia, Anal. Chem. 76 (2004) 6321.
[10] A. Zuttel, P. Wenger, P. Sudan, P. Mauron, S. Orimo, Mater. Sci. Eng., B, Solid 108 (2004) 9.
[11] G. Kolb, R. Zapf, V. Hessel, H. Lowe, Appl. Catal., A 277 (2004) 155.
[12] A. Cabot, J. Arbiol, A. Cornet, J. Morante, F. Chen, M. Liu, Thin Solid Films 436 (2003) 64.
[13] O. Varghese, G. Mor, C. Grimes, M. Paulose, N. Mukherjee, J. Nanosci. Nanotechnol. 4 (2004) 733.
[14] T. Aaltonen, M. Ritala, Y. Tung, Y. Chi, K. Arstila, K. Meinander, M. Leskela, J. Mater. Res. 19 (2004) 3353.
[15] A. Johansson, J. Lu, J. Carlsson, M. Boman, J. Appl. Phys. 96 (2004) 5189.
[16] J.J. Senkevich, F. Tang, D. Rogers, J. Drotar, C. Jezewski, W. Lanford, G. Wang, T. Lu, Chem. Vap. Depos. 9 (2003) 258.
[17] J.J. Senkevich, G. Yang, T. Lu, T. Cale, C. Jezewski, W. Lanford, Chem. Vap. Depos. 8 (2002) 189.
[18] G.A.T. Eyck, J.J. Senkevich, F. Tang, D. Liu, S. Pimanpang, T. Karaback, G.-C. Wang, T.-M. Lu, C. Jezewski, W.A. Lanford, Chem. Vap. Depos. 11 (2005) 60.
[19] Y.-S. Kim, G.A.T. Eyck, D. Ye, C. Jezewski, T. Karabacak, H.-S. Shin, J.J. Senkevich, T.-M. Lu, J. Electrochem. Soc. 152 (2005) C376.
[20] J. Huo, R. Solanki, J. McAndrew, J. Mater. Res. 17 (2002) 2394.
[21] J. Elam, M. Groner, S. George, Rev. Sci. Instrum. 73 (2002) 2981.
[22] M.N. Rocklein, S.M. George, Anal. Chem. 75 (2003) 4975.
[23] G.J.K. Acres, K. Swars, Gmelin Handbook of Inorganic Chemistry, vol. A1, Springer-Verlag, Berlin, 1986, p. 45, Pt Suppl.
[24] H. Masuda, M. Satoh, Jpn. J. Appl. Phys. 35 (1996) L126.
[25] H.H. Wang, C.Y. Han, G.A. Willing, Z. Xiao, Mat. Res. Soc. Symp. Proc. 775 (2003) 107.
[26] J. Elam, D. Routkevitch, P. Mardilovich, S. George, Chem. Mater. 15 (2003) 3507.
[27] M. Juppo, P. Alen, M. Ritala, M. Leskela, Chem. Vap. Depos. 7 (2001) 211.
[28] J. Chae, H.S. Park, S.W. Kang, Electrochem. Solid-State Lett. 5 (2002) C64.
[29] Y.Y. Shacham-Diamond, Electrochem. Solid-State Lett. 3 (2000) 279.
[30] A. Rahtu, T. Alaranta, M. Ritala, Langmuir 17 (2001) 6506.
[31] J.W. Elam, C.E. Nelson, R.K. Grubbs, S.M. George, Thin Solid Films 386 (2001) 41.
[32] F.H. Fabreguette, Z.A. Sechrist, J.W. Elam, S.M. George, Thin Solid Films 488 (2005) 103.
[33] F.R. Hartley, Supported Metal Complexes, Reidel, Dordrecht, 1985.
[34] M. Krawczyk, A. Jablonski, L. Zommer, J. Toth, D. Varga, L. Kover, G. Gergely, M. Menyhard, A. Sulyok, Z. Bendek, B. Gruzza, C. Robert, Surf. Interface Anal. 33 (2002) 23.
[35] J.W. Elam, Z.A. Sechrist, S.M. George, Thin Solid Films 414 (2002) 43.
[36] M.D. Groner, J.W. Elam, F.H. Fabreguette, S.M. George, Thin Solid Films 413 (2002) 186.
[37] J.D. Ferguson, A.W. Weimer, S.M. George, Chem. Mater. 16 (2004) 5602.
[38] R. Matero, A. Rahtu, M. Ritala, M. Leskela, T. Sajavaara, Thin Solid Films 368 (2000) 1.
[39] T. Aaltonen, M. Ritala, T. Sajavaara, J. Keinonen, M. Leskela, Chem. Mater. 15 (2003) 1924.
[40] F. Favier, E.C. Walter, M.P. Zach, T. Benter, R.M. Penner, Science 293 (2001) 2227.
[41] O. Dankert, A. Pundt, Appl. Phys. Lett. 81 (2002) 1618.
[42] Y. Sakamoto, K. Takai, I. Takashima, M. Imada, J. Phys., Condens. Matter 8 (1996) 3399.